ATLAS

P. Albicocco, M. Antonelli(Resp.), M.M. Beretta, H. Bilokon,
S. Cerioni, V. Chiarella, M. Curatolo, R. Di Nardo,
M. Dreucci, B. Esposito, C. Gatti, P.F. Laurelli,
G. Maccarrone, A. Martini, G. Mancini, G. Pileggi (Tech.),
B. Ponzio(Tech.), V. Russo(Tech.), A. Sansoni,
M. Testa, T. Vassilieva (Tech.), E. Vilucchi.

In collaboration with
Centro di Calcolo:
M. Pistoni, D. Spigone Metrologia Divisione Acceleratori:
S. Lauciani, M. Paris, F. Putino

April 6, 2017

1 Higgs boson properties in the $H \to ZZ^* \to 4l$ decay channel

In the 2015 and 2016 data taking at LHC, ATLAS collected proton-proton collisions at 13 TeV center of mass energy, corresponding to an integrated luminosity of 14.8 fb^{-1}.
Back on 4 July, 2012, the LHC experiments reported the evidence of an Higgs boson-like particle with a mass of about of 125 GeV and great interest has been posed on the measurements of its properties to assure whether it is the Standard Model (SM) Higgs boson or not. In this context, during the Run2 at LHC, with an increased center of mass energy of the collisions, the measurement of the Higgs properties remains one of the main goals of the physics program since hints of New Physics (NP) effects can be hidden in the Higgs sector. Deviations from the SM expectations could indicate exotic properties of the Higgs or presence of exotic particles in association with Higgs.
Studies performed during Run1 showed that deviations from the SM expectations in the Higgs sector are small: the Higgs quantum numbers are measured to be $J^P = 0^+$ (alternative hypotheses are excluded with a 99.9% C.L.), its signal strength ($\mu = Ev_{obs}/Ev_{SM}$) and coupling measurements to vector bosons and fermions are found to be consistent with the SM with an accuracy of the order of 10%.
In the $H \to ZZ^* \to 4\ell$ final state, the first measurement in Run2 have been focusing on the Higgs boson coupling to SM particles. The measurement has been performed dividing the events in categories built depending on the characteristic of the event, aiming for discrimination between production modes. The measurement of the cross section per production mode has been performed, together with the measurement of the Higgs boson couplings to bosons and fermions.
In the SM, the Higgs boson is a $\mathcal{CP}$-even scalar particle ($J^{\mathcal{CP}} = 0^{++}$) and theories of physics BSM often require an extended Higgs sector featuring several neutral Higgs bosons. Such cases may include $\mathcal{CP}$-mixing in the Higgs boson interactions, which could result in observable differences in the kinematics of final-state particles produced in their decays, or from Higgs boson production, such as in VBF interactions.
The possible presence of BSM terms in the Lagrangian describing the spin-0 resonance is investigated describing the HVV vertex interaction in terms of an effective BSM $\mathcal{CP}$-odd and $\mathcal{CP}$-even operators and deriving limits on the corresponding BSM tensor couplings are derived. Our group contributed significantly to this studies ([1]) with fundamental contributions to the analysis and to the measurement of the Higgs boson properties in the $H \to ZZ^* \to 4\ell$ decay channel.

1.1 Cross section per production mode measurements

In order to measure the cross sections per production mode, categories enriched in each Higgs production mechanism have been defined 1. Five categories have been defined depending on the event characteristics and on the number of jets associated to the event, as shown in Figure 1:

- VH-leptonic-enriched: requiring an additional lepton in the event ($p_{T,\ell} > 8$ GeV),
- 0-jet: $N_{\text{jets}} = 0$,
- 1-jet: $N_{\text{jets}} = 1$ ($p_{T,jet} > 30$ GeV),
- 2-jet VBF-enriched: $N_{\text{jets}} \geq 2$, $m_{jj} > 120$ GeV ($p_{T,jet} > 30$ GeV),
- 2-jet VH-hadronic enriched: $N_{\text{jets}} \geq 2$, $m_{jj} < 120$ GeV ($p_{T,jet} > 30$ GeV).

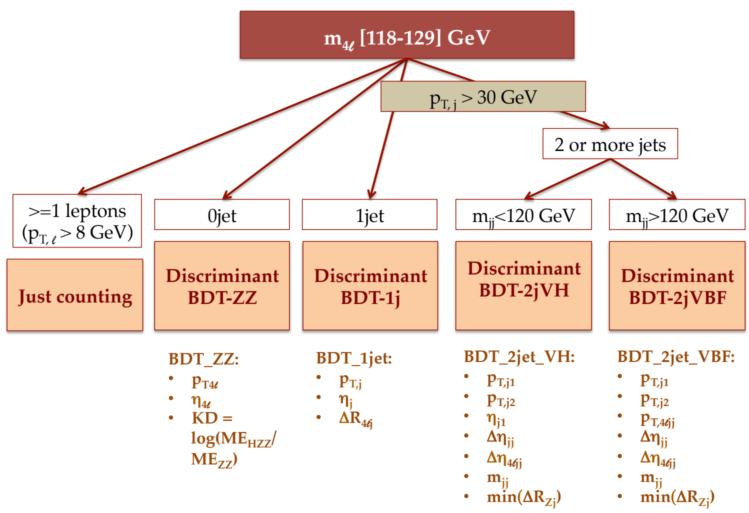

Figure 1: Event categorization scheme.

Multivariate discriminants have been defined in each category in order to discriminate the signal contribution among the backgrounds. Figure 2 shows the fraction of signal events in each category per production modes, showing the extreme purity of some categories. The relation between N_k^{obs}, the observed number of events in each analysis categories (denoted as k), and the

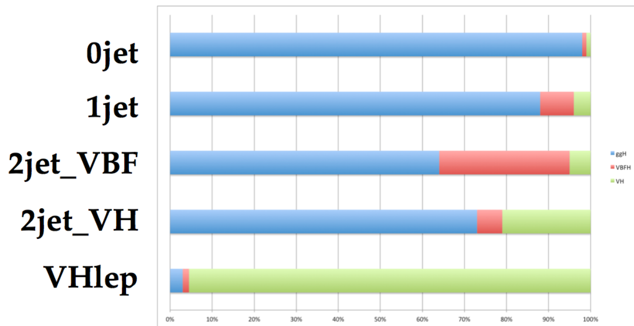

Figure 2: Fraction of events per production mode and per category.

cross section in each truth bin σ_i^j (i denotes different production mechanisms and j denotes the index of a phase space or truth bin in the simplified template cross section binning scheme), can be expressed as follows:

$$\mathcal{N}_k^{\text{obs}} = \mathcal{L}_{\text{int}} \times \mathcal{BR}_{H\to ZZ^*\to 4\ell} \times \left(\sum_{i=1}^{\mathcal{N}^{prod}} \sum_{j=1}^{\mathcal{N}_{bin}^i} \mathcal{A}_{kj}^i \sigma_i^j \right) \tag{1}$$

where $\mathcal{L}_{\text{int}}$ is the integrated luminosity, $\mathcal{N}^{prod}$ is the number of Higgs production mechanisms, $\mathcal{N}_{bin}^i$ is the number of truth bins per Higgs production mechanism i, $\mathcal{A}_{kj}^i$ takes into account for detector response (trigger, reconstruction and identification efficiencies) for detecting the final state and the kinematic and geometric acceptance for the truth bin j of Higgs production mechanism i in the analysis category k.
Results are extracted from fits to the data using the profile likelihood ratio: Table 1 reports the expected and observed number of events.
Figure 3 and Table 2 show the results in terms of cross sections per production mode.

Table 1: Expected and observed yields in the 0-jet, 1-jet, 2-jet with $m_{jj} > 120$ GeV (VBF-*enriched*), 2-jet with $m_{jj} < 120$ GeV (VH-*enriched*) and VH-leptonic categories. The yields are given for the different production modes, assuming $m_H = 125$ GeV, the ZZ^* and reducible background for $14.8 fb^{-1}$ at $\sqrt{s} = 13$ TeV. The estimates are given for the $m_{4\ell}$ mass range 118–129 GeV.

Analysis	Signal				Background		Total	Observed
category	ggF + $b\bar{b}H$ + $t\bar{t}H$	VBF	WH	ZH	ZZ^*	Z + jets, $t\bar{t}$	expected	
0-jet	11.2 ± 1.4	0.120 ± 0.019	0.047 ± 0.007	0.060 ± 0.006	6.2 ± 0.6	0.84 ± 0.12	18.4 ± 1.6	21
1-jet	5.7 ± 2.4	0.59 ± 0.05	0.137 ± 0.012	0.091 ± 0.008	1.62 ± 0.21	0.44 ± 0.07	8.5 ± 2.4	12
2-jet VH enriched	1.1 ± 0.5	0.084 ± 0.009	0.143 ± 0.012	0.101 ± 0.009	0.166 ± 0.035	0.088 ± 0.011	1.6 ± 0.5	2
2-jet VBF enriched	1.9 ± 0.9	0.92 ± 0.07	0.074 ± 0.007	0.052 ± 0.005	0.22 ± 0.05	0.24 ± 0.11	3.4 ± 0.9	9
VH-leptonic	0.055 ± 0.004	0.00217 ± 0.00015	0.067 ± 0.004	0.0105 ± 0.0006	0.0156 ± 0.0015	0.012 ± 0.010	0.163 ± 0.012	0
Total	20 ± 4	1.71 ± 0.14	0.47 ± 0.04	0.315 ± 0.027	8.2 ± 0.9	1.62 ± 0.07	32 ± 4	44

The same categorization can be used for the measurements of coupling modifiers (κ) to SM particles within the k-framework interpretation. Figure 4

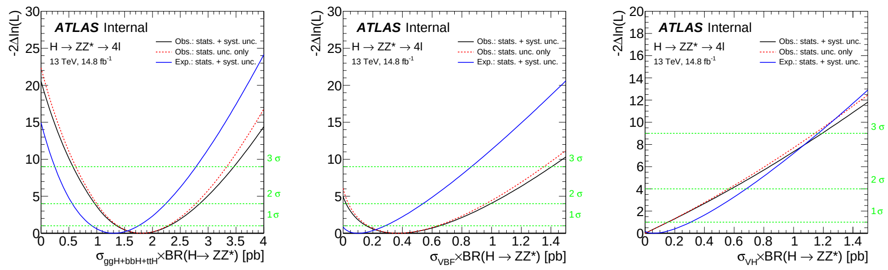

Figure 3: NLL scan results for $L_{int} = 14.8 fb^{-1}$ of $\sqrt{s} = 13$ TeV data.

Table 2: The expected and observed cross section per production mode results ($(\sigma \times \mathcal{BR})^{ZZ}_{ggH+bbH+ttH}$, $(\sigma \times \mathcal{BR})^{ZZ}_{VBF}$, $(\sigma \times \mathcal{BR})^{ZZ}_{VH}$), for $14.8 fb^{-1}$ at $\sqrt{s} = 13$ TeV.

Production process	Expected (pb)	Observed (no syst., pb)	Observed (with syst., pb)
$(\sigma \times \mathcal{BR})^{ZZ}_{ggH+bbH+ttH}$	1.31 $\pm$ 0.07	$1.80^{+0.47}_{-0.42}$	$1.80^{+0.49}_{-0.44}$
$(\sigma \times \mathcal{BR})^{ZZ}_{VBF}$	0.100 $\pm$ 0.003	$0.37^{+0.27}_{-0.20}$	$0.37^{+0.28}_{-0.21}$
$(\sigma \times \mathcal{BR})^{ZZ}_{VH}$	0.059 $\pm$ 0.002	$0^{+0.15}$	$0^{+0.15}$

shows the interpretation in terms of coupling modifiers of the Higgs boson coupling to fermions (κ_f) and vector bosons (κ_V).

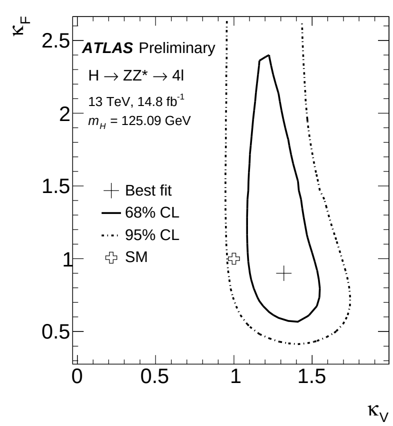

Figure 4: 2D likelihood scan of the κ_V and κ_F.

1.1.1 Effective Field Theory (EFT) interpretation

This study aims to use properties from the different production mechanisms and the $H \to ZZ^*$ decays to derive information on the $\mathcal{CP}$ nature of the Higgs boson.
Due to the fact that the VBF and VH production mechanisms are particularly sensitive to possible BSM contributions, an effective field theory (EFT) approach has been adopted in order to describe the interactions between the resonance and the SM vector bosons, following the Higgs boson characterisation model [3] [2].
Among all the possible scenarios, only the hypothesis that the observed resonance is a mixture of spin-0 $\mathcal{CP}$-even and/or $\mathcal{CP}$-odd states has been considered, meaning that, in the case of $\mathcal{CP}$ mixing, the Higgs boson would be a mass eigenstate, but not a $\mathcal{CP}$ eigenstate, implying $\mathcal{CP}$-violation in the Higgs sector.
In all cases, only one resonance with a mass of about 125 GeV is considered; it is also assumed that the total width of the resonance is small with respect to the typical experimental resolution of the ATLAS detector and the interference effects between the signal and SM backgrounds are negligible.
The Higgs Characterization model relies on an EFT approach which, by definition is only valid up to a certain energy scale Λ, set to 1 TeV to account for the experimental results obtained by the LHC and previous collider experiments that show no evidence of new physics at lower energy scales.
The model assumes that the resonance structure corresponds to one new boson, assuming that any other BSM particle exists at an energy scale larger than Λ.
The investigation of possible mixing between the Standard Model $\mathcal{CP}$-even and BSM $\mathcal{CP}$-even and $\mathcal{CP}$-odd contributions is performed, providing a study of the HVV Lagrangian tensor structure.
In the Higgs boson characterization model, the description of the spin-0 particle interaction with pairs of W and Z bosons is given through the following interaction Lagrangian:

$$\begin{aligned}\mathcal{L}_0^V = \quad & \Big\{ c_\alpha \kappa_{\mathrm{SM}} \left[\tfrac{1}{2} g_{HZZ} Z_\mu Z^\mu + g_{HWW} W_\mu^+ W^{-\mu}\right] \\ & -\tfrac{1}{4}\tfrac{1}{\Lambda}\left[c_\alpha \kappa_{HZZ} Z_{\mu\nu} Z^{\mu\nu} + s_\alpha \kappa_{AZZ} Z_{\mu\nu}\tilde{Z}^{\mu\nu}\right] \\ & -\tfrac{1}{2}\tfrac{1}{\Lambda}\left[c_\alpha \kappa_{HWW} W^+_{\mu\nu} W^{-\mu\nu} + s_\alpha \kappa_{AWW} W^+_{\mu\nu}\tilde{W}^{-\mu\nu}\right]\Big\} X_0.\end{aligned} \tag{2}$$

where V^μ represents the vector-boson field ($V = Z, W^\pm$), the $V^{\mu\nu}$ are the reduced field tensors and the dual tensor is defined as $\tilde{V}^{\mu\nu} = \frac{1}{2}\varepsilon^{\mu\nu\rho\sigma}V_{\rho\sigma}$. The κ_{SM}, κ_{HVV} and κ_{AVV} denote the coupling constants corresponding to the interaction of Standard Model, BSM $\mathcal{CP}$-even and BSM $\mathcal{CP}$-odd spin-0 particles, represented by the X_0 field, with ZZ or WW pairs.
Other higher-order operators [2], namely the derivative operators, are not included in Equation 2 and have been neglected in this analysis. To ensure that the Lagrangian terms are Hermitian, these couplings are assumed to be

real.
The mixing angle α allows for production of $\mathcal{CP}$-mixed states and implies $\mathcal{CP}$-violation for $\alpha \neq 0$ and $\alpha \neq \pi$, provided the corresponding coupling constants are non-vanishing: the following notation will be used hereafter: $s_\alpha = \sin\alpha$ and $c_\alpha = \cos\alpha$.
The Standard Model coupling strengths, g_{HVV}, are proportional to the square of the vector boson masses: $g_{HVV} \propto m^2_{Z/W}$.
To quantify the presence of BSM contributions in experimentally observed $H \rightarrow ZZ^*$ decay, the observed ratios of couplings κ_{AVV} and κ_{HVV} are measured for the $\mathcal{CP}$-mixing and anomalous $\mathcal{CP}$-even contribution scenarios, respectively.
All the models used in these studies are obtained by selecting the corresponding parts of the Lagrangian described in Equation 2 while setting all other contributions to zero. The custodial symmetry has been also imposed: in κ_{AVV} and κ_{HVV} $V = W, Z$.
The BSM terms described in Equation 2 are also expected to change the relative contributions of the vector-boson fusion (VBF) and vector-boson associated production (VH) processes with respect to the gluon-fusion (ggF) production process, which is predicted to be the main production mode for the SM Higgs boson at the LHC.
For large values of the BSM couplings, the VBF and VH production modes can have a significantly higher cross section due to the fact that the BSM couplings to W/Z bosons enter with the square power in the computation of the cross section. For the VBF and VH Higgs boson events decaying into 4ℓ final state the contribution of κ_{BSM} enters both in production and decay vertexes; while for the ggH, ttH and bbH, κ_{HVV} and κ_{AVV} can only enter in the decay vertex as shown in Figure 5. The expected results for the tensor

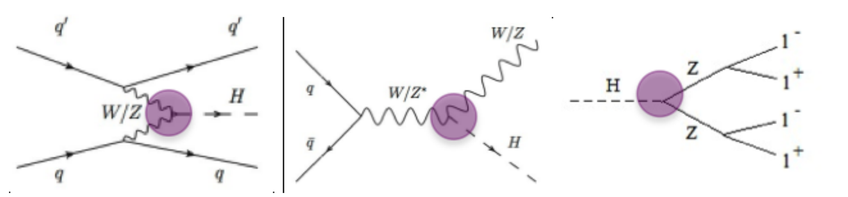

Figure 5: Interaction vertices involving the κ_{HVV} and κ_{AVV} BSM coupling considered.

coupling analysis are obtained using an Asimov data set built from Standard Model events. The tensor couplings have been studied separately, fixing in the Lagrangian the SM component to its expectation ($\kappa_{SM} = 1$).
The likelihood expected distribution of Figure 6 is symmetric since the cross section scales at the same rate for negative and positive values of κ_{AVV}; a small asymmetry is therefore seen due to the difference in the categorization among positive and negative values of κ_{AVV}. Table 3 shows a comparison between the observed and expected limits at 95% CL for the tensor couplings

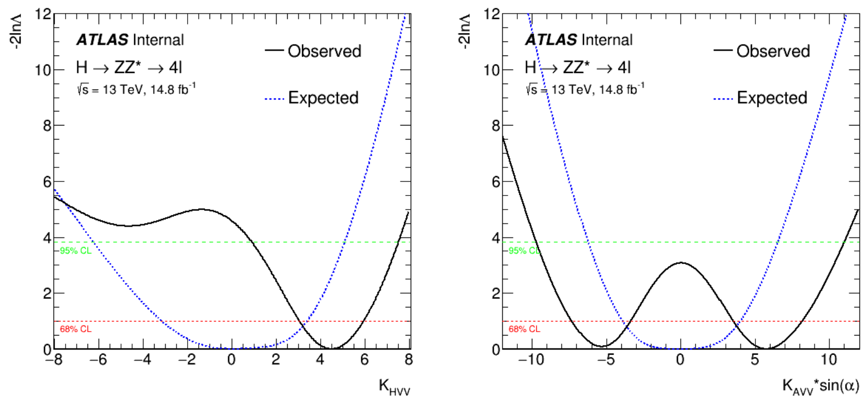

Figure 6: Observed (black) and expected (blue) results for the κ_{HVV} (left) and κ_{AVV} (right) analysis of the tensor coupling structure of the Higgs Boson.

chosen in this analysis.

Table 3: Comparison among the Observed and Expected exclusion limits with the Run2 data set.

Expected not excluded range at 95% CL	κ_{HVV}	$\kappa_{AVV} \times \sin(\alpha)$
Run 2 dataset	$[-6.25, 5.05]$	$[-6.25, 6.5]$
Observed not excluded range at 95% CL	κ_{HVV}	$\kappa_{AVV} \times \sin(\alpha)$
Run 2 dataset	$[0.9, 7.45]$	$[-9.7, 11.0]$

2 Jet and Missing Transverse Energy reconstruction

2.1 Particle Flow Reconstruction and PileUp suppression

The increase of luminosity expected for RunII, to up to 80 mean interaction per bunch crossing, will induce serious degradation of the jets and $\not{E}_T$ resolutions and increase in fake rate contamination from Pileup jets. Standard ATLAS reconstruction exploits several techniques to mitigate Pileup effects in the jets and in the $\not{E}_T$ reconstruction. These techniques are aimed to improve resolution and reduce the fake rate of jet and $\not{E}_T$. One well established approach is calorimeter based and uses the "Jet Area" method[4], which basically evaluates the average energy Pileup contribution under the area of the jet and subtract it. This approach has the intrinsic limitation to not be able to capture local Pileup fluctuations, limiting therefore the resolution improvements and the rejection of Pileup jets. Other local approaches based on tracks have been develop to reduce Pileup jets rate. They exploit the possibility of extrapolating the tracks to the interaction vertex and therefore to identify a signal jet coming from the hard scatter vertex from the Pileup Jets coming from other Pileup vertices[5]. Even if those techniques are track-based, the constituents of the jets are calorimeter clusters. Therefore, no improvement in the resolution of jets is expected and signal jets will still suffer resolution degradation from Pileup contamination. To face the future unprecedented Pileup conditions a Particle-Flow reconstruction has been revisited and developed within the collaboration. A paper is close to be published [6]. This kind of reconstruction can maximally mitigate Pileup effects by exploiting the correlations among the inner detector and the calorimeter. Through the association between tracks and calorimeter deposits and the track pointing to the interactions vertices, calorimeter energy deposits coming from Pileup interactions can be removed in the jets and $\not{E}_T$ reconstruction. Large improvements in resolutions and fake rate reduction can be therefore achieved.

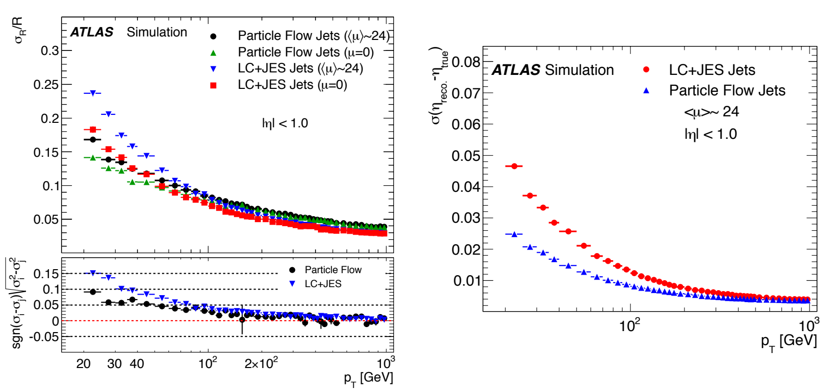

Figure 7: Left: The resolutions of calorimeter and particle flow jets determined as a function of p_{T} in Monte Carlo dijet simulation, compared with no pile-up and conditions similar to 2012 running. The quadratic difference in the resolution with and without pile-up is shown in the lower panel. Right: the angular resolution measured in Monte Carlo by fitting Gaussian functions to the difference between the truth and reconstructed quantities.

Figure 7 (left) shows the fractional p_T resolution of calorimeter based standard jets and Particle-Flow jets, with no pile-up and conditions similar to 2012 running. The right plot of figure 7 shows the resolution on the η direction versus the truth p_T of the jet. The algorithm has been integrated into the ATLAS software framework for Run 2 and is now available for use in physics analyses.

2.2 Jet/Etmiss studies with ITk for Phase-II upgrade

After the "Phase-I" upgrade in 2018, the LHC will undergo a "Phase-II" upgrade in 2023, to deliver the instantaneous luminosity of $\sim 7.5 \times 10^{34} cm^{-2} s^{-1}$, more than a factor 10 beyond its design value, corresponding to unprecedented PileUp conditions with an a average of 200 interactions per crossing. The ATLAS detector will undergoes upgrades to maintain its capabilities. In particular the Inner Detector (ID) will be substituted by a new, all-silicon Inner Tracker (ITk) [7].
Simulation Studies [8] are on going to evaluate the best layout, whose acceptance will be up to $|\eta|$ =4.0 (current ID extends up to $|\eta|$ =2.7). The two layouts under consideration, "Extended Layout" and "Inclined Layout" differ mostly in the forward region.
There is tremendous potential for improved performance for jets and $\not{E}_T$ in the very forward region. Tracking information can be used by tagging pile-up jets in the forward region as has been done in the central region for Run I. Forward pile-up rejection induces an improvement in $\not{E}_T$ as well.
Therefore performances of the Jet and $\not{E}_T$ reconstruction are a key quantity to address the best coiche of the ITk layout.
The variable used to study the forward pile-up jet tagging is $R_{pT} = \frac{\Sigma_k p_T^{trk_k}(PV_0)}{p_T^{jet}}$ which computes the scalar sum of the p_T of the charged tracks associated with a particular jet, which are also associated with the primary vertex (PV0), and normalizes this to the p_T of the relevant jet. Small values of R_{pT} correspond to jets with very small charged fraction associated with the primary vertex, and hence very likely to be pileup jet. The efficiency of the R_{pT} cut for hard-scatter jets versus the efficiency for pile-up jets is shown in Figure 8, left, where each curve represents a scan over the observable R_{pT} for jets in a range of $|\eta|$.
The $\not{E}_T$ resolution derived from fully simulated $t\bar{t}$ events with average $\mu =$ 200 as a function of ΣE_T is shown in Figure 8, right, for the two layouts. The results shown here indicate that with the Inclined Layout better performances on the jet and $\not{E}_T$ reconstruction can be achieved. This results is driven by the better track z_0 resolution at low momentum (O(1 GeV)) with the Inclined Layout. More information are in [8].

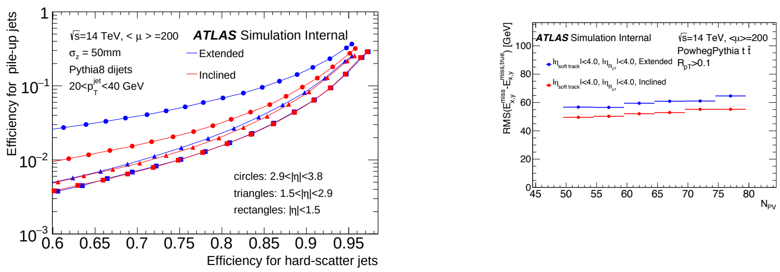

Figure 8: Left: The efficiency for pile-up jets as a function of the efficiency for hard-scatter jets with $20 < p_{\mathrm{T}} <$40 GeV using a track-matching algorithm for $\mu = 200$. Right: The resolutions of the x and y components of $\not{E}_T$ for samples of $t\bar{t}$ events with $\mu = 200$ as a function of the scalar sum of total energy in the event. Results are shown for the in the Extended and Inclined Layouts.

3 New Small Wheel upgrade project: MicroMegas

In the year 2016 the R&D process on the MicroMegas (MM) detector, the phase-1 upgrade of the ATLAS Forward Muon Spectrometer, arrived to a conclusion with the Module 0 construction (Figure 9).

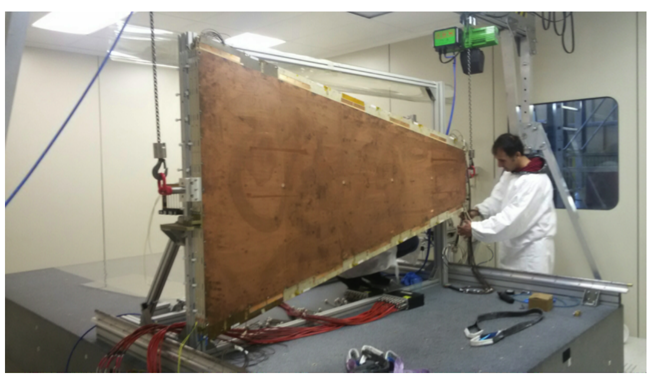

Figure 9: Completed Module 0 ready to be removed from the assembly tool.

The INFN collaboration, responsible for the SM1 chambers, built the Module 0 in April-May and, tran sported at CERN, tested in a high energy muon/pion SPS secondary beam (H8) (Figure 10).
The Italian MM group was the only one able to build their own Module 0 in the year 2016, the other three groups will do it in 2017.
Test results were satisfactory, resolution, both in precise coordinate and in the

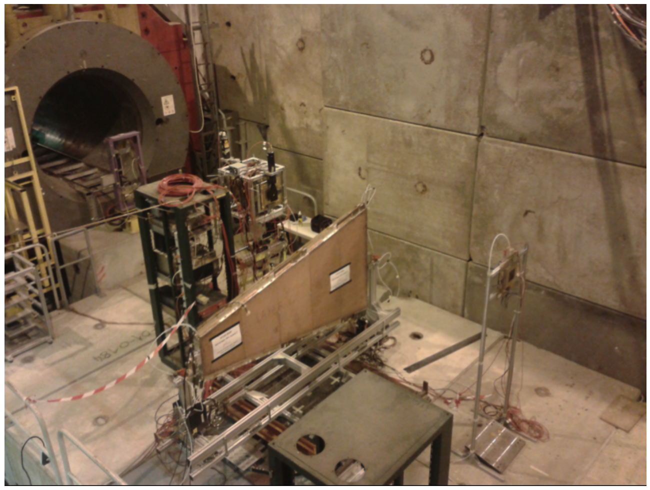

Figure 10: Test beam setup in the H8 SPS beam line, with SM1 Module 0.

second coordina te, was close to the expectations, as the efficiency (Figure 11 and 12).

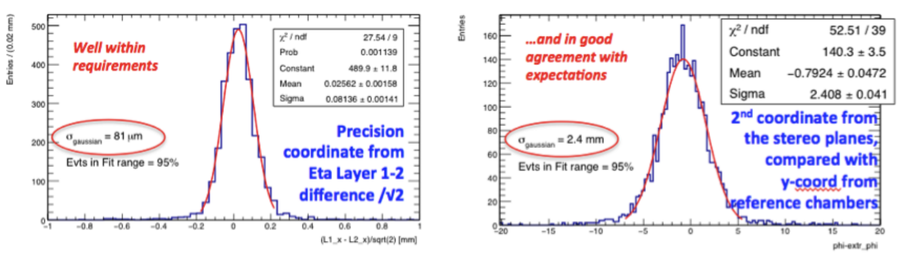

Figure 11: Module 0 resolutions obtained in the test beam.

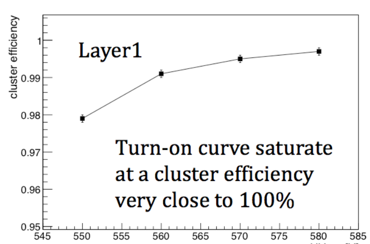

Figure 12: Turn On curve, efficiency Vs HV showing good efficiency, close to 1.

A preliminary test of the PCB precision alignment in the relevant coordinate

show a result that is not fully satisfactory but well in line with the mechanical precision in the PCB construction, that must be improved for the serial production.
Test of mechanical integration of the SM1 Module 0 was also performed at CERN, showing that the d etector is from the mechanical point of view even more stiff than foreseen in the simulation (Figure 13).

Figure 13: Mechanical simulation of the SM1 mounting in the Whell. The yellow/black structure provide d detector rotation in all possible final positions.

The module 0 went back to LNF in September to be re-opened to study in details the reasons for some HV instability seen during the test beam.
After this work, at the end of the year, many unstable sectors were fixed and the number of resid ual problematic ones was of the order of 10% related to the poor single PCB quality.

4 FTK

The trigger is a fundamental part of any experiment at hadron colliders. It is needed to select on-line the interesting low cross-section physics from the huge QCD background. Experience at high luminosity hadron collider experiments shows that controlling trigger rates at high instantaneous luminosity can be extremely challenging. As the luminosity increases, physics goals change in response to new discoveries, and detector ageing. It is thus essential that the trigger system be flexible and robust, and redundant and significant operating margin. Providing high quality track reconstruction over the full ATLAS Inner Detector by the start of processing in the level-2 computer farm can be

an important element in achieving these goals. With the goal to improve and make more robust the ATLAS trigger, during summer 2007 the group joined the Fast-Track (FTK) proposal for A hardware track finder for the ATLAS trigger. This is a proposal to build a hardware track finder as an upgrade to the ATLAS trigger. It will provide global reconstruction of tracks above 1 GeV/c in the silicon detectors, with high quality helix parameters, by the beginning of level-2 trigger processing. FTK can be particularly important for the selection of 3rd-generation fermions (b and τ). These have enormous background from QCD jets, which can be quickly rejected in level-2 if reconstructed tracks are available early. This RD proposal was completed with the submission of the FTK Technical Proposal that was finally approved by the ATLAS collaboration meeting in June 2011.
Under the FTK context we contributed in the development and test of the Associative Memory (AM) chips for track detection and the FTK Input Mezzanines (IMs) boards for hit information clustering.

4.1 FTK Input Mezzanines

The FTK IMs boards receive data to be processed from the detectors Read Out Drivers (RODs) over 380 S-Link for a total input rate of $760Gbps$. Each board receives data over four optical links at $2Gbps$, performs an early reduction of the data to optimize the subsequent FTK processing and transmits forward the clustered data by a $200MHz\ DDR$ signalling over 16 LVDS pairs.
Due to the high occupancy of the IBL ATLAS pixel layer, the previous version of the FTK IM board based on Xilinx Spartan6 FPGA could not process all the data coming from the detector. We have developed this board together with FTK Japanese group of Waseda University. As responsible of this board the FTK collaboration ask us to develop a new version of the FTK IM based on a Xilinx Artix7 FPGA. This is a more recent and powerfull FPGA.
The new board have been designed in 2014, Figure 14.
During 2015 the first prototype has been fully tested and 80 boards have been produced, tested and delivered to CERN.
During 2016 the firmware of the Artix-7 IM has been constantly kept updated with the firmware of the Spartan6 version. The main activities are reported in the following.
Timing errors in the Artix-7 IM firmware have been fixed every time they appeared subsequently to new firmware update.
The Spartan6 IM firmware sometimes failed to recover after a remote reset. This issue has been investigated and solved.
There was the need to expand the possibility of testing the FTK data flow with a set of pseudo-data larger than the one implemented in the firmware. An interface to an on-board SRAM memory has been developed for this purpose allowing to save up to 512K samples per each of the two channels of

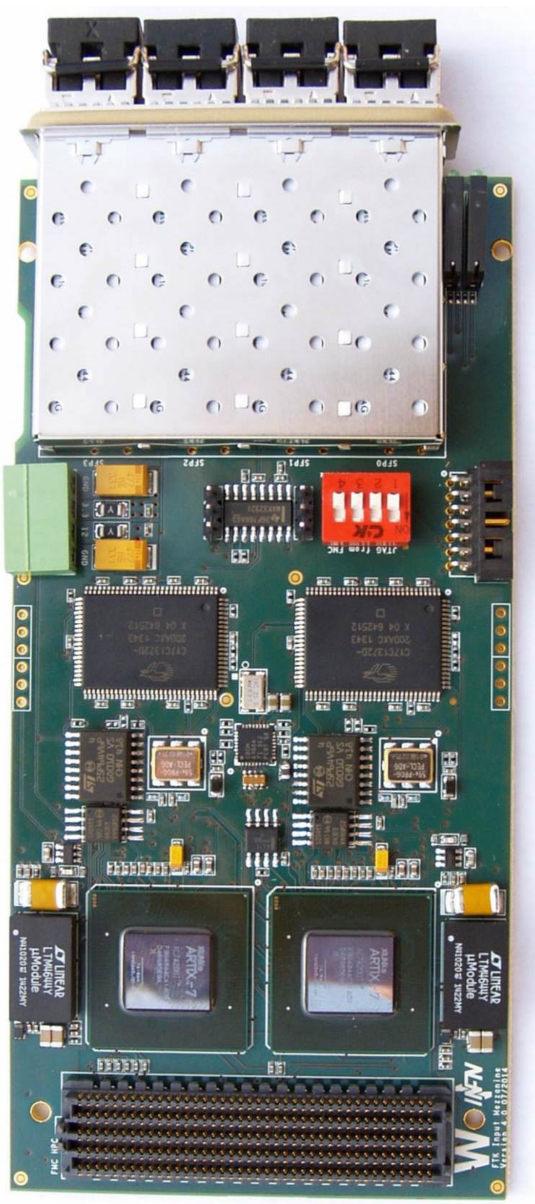

Figure 14: Artix7-IM

each mezzanine. The pseudo-data can be read back from the memory at the maximum rate of 160 Msps.

4.2 FTK AMCHIP06 test

In 2016 was completed the AMchip06 pre-production test at Microtest. LNF is involved in the test of this chip with these items:

- design a new test board without low drop voltage regulator;
- organizing and following the mass production test with external company.

In the following paragraph the listed items will be described.

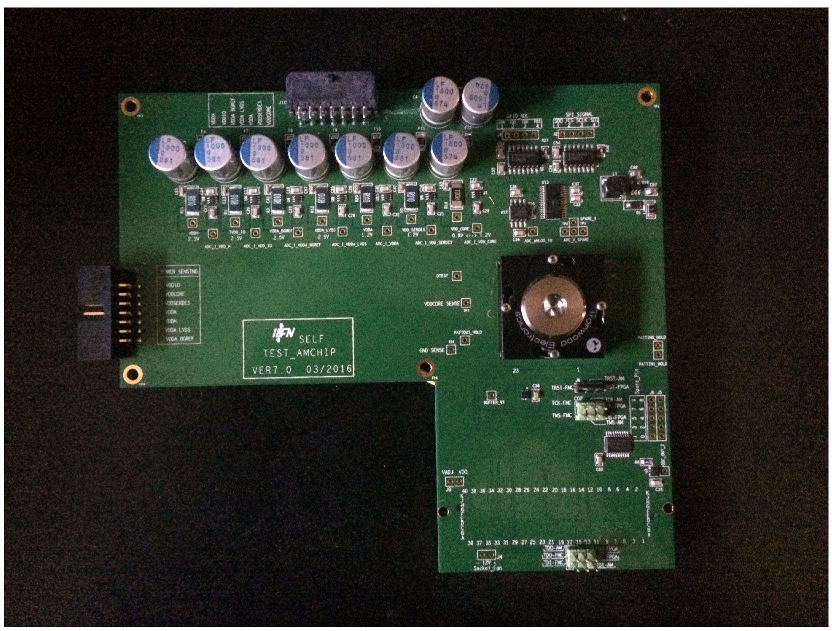

Figure 15: New test board for the AMchip06

The test board for the Amchip06 is designed to be compatible with the standard FMC connectors hosted on Xilinx evaluation board. This because the firmware that controls the tests is implemented in Xilinx Virtex6 FPGA. The specification used to design the board was the following:

- FMC HPC connector
- On Board 100MHz clock
- FMC alternative clock distribution

- 12 differencial high speed (2.5 GHz) lines
- On board power supply current and voltage monitor

The board designed with all features highlighted are shown in the picture 15
We have produced, tested and distributed to the various test site the new test boards.
LNF FTK group is in charge to follow the tender for the test of the AMchip06 production. The company choose for test the chip is Microtest. We have visited the company and agree with them about the test procedure and the installation of the test stand in their laboratories in 2016. We have installed the test equipment to the company laboratory and we have trained the personel in charge of the test. The test last three from october to december 2016. The results of these tests shows a yeld of more than 80% in the AMchip06 pre-production.
Tests of mass production will be start in the beginning of 2017.

5 Tier-2

During the year 2016 the Frascati Tier-2 successfully and continuously performed all the typical activities of an ATLAS Tier-2: Monte Carlo production and users and physics groups analysis; the efficiency of the site was always maintained above 90%.
During the year, the Tier-2 farm has grown to 17 kHEPSPEC of computing power and about 1.2 PB of disk space. Supported Virtual Organizations (VO) are: LHC VOs, Belle, CTA and KM3Net.
Among the most significant activities that involved the Tier-2 staff we can mention the role of VO manager for ATLAS VO and software VO manager for KM3Net VO. This activities are of primary importance for the experiments, in fact, one of them is also recognized as in kind contribution of the Italian group.
Finally, for what concern the Grid middleware, during 2016 the Tier-2 The Tier-2 continued to host the testbed of the DPM service (Disk Pool Manager) for the DPM international collaboration, regularly testing the updates and experimenting new technologies (such as HTTP Federation) before to propose them to the experiments.

Public presentations:

- G.Mancini, "EFT approach for the Higgs physics at LHC", Talk at the XII ATLAS-Italy Workshop on Physics and Upgrade, 23rd-25th November 2016.
- G.Mancini, "Studio dei meccanismi di produzione del bosone di Higgs nel canale di decadimento $H \to ZZ^* \to 4l$ a $\sqrt{s} = 13$ TeV con il

detector ATLAS ad LHC", Talk at the 102° SIF congress (Congresso della Societá Italiana di Fisica (SIF)), 26th-30th September 2016.

- G.Mancini, "Study of the Higgs boson properties and search for high-mass scalar resonances in the $H \rightarrow ZZ^* \rightarrow 4l$ decay channel", Talk at the ATLAS Physics Plenary for the Approval of the CONF Note CONF-HIGG-2016-16 (on behalf of the $H \rightarrow ZZ^* \rightarrow 4l$ group), 26th July 2016.
- G.Mancini, "Review sulle proprietá del bosone di Higgs negli esperimenti ATLAS e CMS ad LHC", Talk at the italian workshop on the pp Physics at LHC (pp LHC 2016), 16th-18th May 2016.
- G.Mancini, "Couplings and simplified cross section measurements for RunII", Talk at the ATLAS Higgs-ZZ group workshop 2016, 26th-29th April 2016.

Publications and internal documents:

- G.Mancini, "Study of the Higgs boson properties and search for high-mass scalar resonances in the $H \rightarrow ZZ^* \rightarrow 4l$ decay channel at $\sqrt{s} = 13$ TeV with the ATLAS detector", ATLAS-COM-CONF-2016-079.
- G.Mancini, "Senstivity studies based on the EFT parametrization in the double differential cross section for the $H \rightarrow ZZ^* \rightarrow 4l$ decay channel at LHC", IL NUOVO CIMENTO Vol. 39 C, 2016 (DOI: 10.1393/ncc/i2016-16210-5, Colloquia: IFAE 2015), 1st July 2016.
- G.Mancini, "Overview of the Higgs boson property studies at the LHC", Proceedings of Science (PP LHC 2016) (publishing)
- C.Gemme et al, "Final Report of the ITk Layout Task Force", ATL-COM-UPGRADE-2016-042
- I.Gregor et al, "Technical Design Report for the ATLAS ITk- Strips Detector", ATL-COM-UPGRADE-2016-035
- A. Henriques at al, "HGTD chapter of the Phase-II Upgrade of the LAr Calorimeter System IDR" , ATL-COM-LARG-2016-045
- ATLAS Collaboration, "Search for long-lived neutral particles decaying into displaced lepton-jets in proton-proton collisions at $\sqrt{s} = 13$ TeV with the ATLAS detector", ATLAS-CONF-2016-042
- M. Testa *et al.*, sFCal plots, https://twiki.cern.ch/twiki/bin/view/AtlasPublic/LArCaloPublicResultsUpgrade
- M. Testa et al, "Jet/EtMiss plots for luminous region studies for ECFA 2016", https://atlas.web.cern.ch/Atlas/GROUPS/PHYSICS/PLOTS/JETM-2016-013/

Responsabilities in ATLAS

R. Di Nardo, Convener of Higgs ZZ working group (2015-2016)

G. Maccarrone, Responsible of the NSW Italian group

M. Testa, Convener of the Missing Transverse Energy reconstruction group (April 2016 - April 2017)

M. Testa, Convener of the Higgs Prospects analysis group (April 2017 - April 2018)

M. Testa, Responsible of the Data Quality of the Missing Transverse Energy offline reconstruction

References

[1] ATLAS Collaboration, Study of the Higgs boson properties and search for high-mass scalar resonances in the $H \to ZZ^* \to 4l$ decay channel at $\sqrt{s} = 13$ TeV with the ATLAS detector, ATLAS-COM-CONF-2016-079.

[2] F. Maltoni, K. Mawatari and M. Zaro, Higgs characterisation via vector-boson fusion and associated production: NLO and parton-shower effects, Eur. Phys. J. C74 (2014) 2710, arXiv: 1311.1829 [hep-ph].

[3] Handbook of LHC Higgs Cross Sections: 4. Deciphering the Nature of the Higgs Sector (arXiv:1610.07922).

[4] M.Cacciari and G.P.Salam, "PileUp subtraction using jet areas", Phys.Lett.B659 (2008) 119-126

[5] ATLAS Collaboration, "Tagging and suppression of pileup jets with the ATLAS detector", ATLAS-CONF-2014-018

[6] ATLAS Collaboration, "Jet reconstruction and performance using particle flow with the ATLAS Detector", submitted to Eur. Phys. J C, http://arxiv.org/abs/1703.10485

[7] ATLAS Collaboration, "Initial Design Report of the ITk", ATL-COM-UPGRADE-2014-029

[8] C.Gemme et al, "Final Report of the ITk Layout Task Force", ATL-COM-UPGRADE-2016-042